Lateral Charge Migration in 1D Semiconductor-Metal Hybrid Photocatalytic Systems

Mathias Micheel,[1] Kaituo Dong,[2] Lilac Amirav,[2*] and Maria Wächtler[1,3*]

[1] *Department Functional Interfaces, Leibniz-Institute of Photonic Technology Jena, Albert-Einstein-Straße 9, 07745 Jena, Germany*
[2] *Schulich Faculty of Chemistry, The Russell Berrie Nanotechnology Institute, The Nancy and Stephen Grand Technion Energy Program, Technion − Israel Institute of Technology, Haifa 32000, Israel*
[3] *Chemistry Department and State Research Center Optimas, RPTU Kaiserslautern-Landau, Erwin-Schrödinger-Straße 52, 67663 Kaiserslautern, Germany*

*Corresponding authors: lilac@technion.ac.il, waechtler@chemie.uni-kl.de

ABSTRACT

Colloidal nanorods based on CdS or CdSe functionalized with metal particles have proven to be efficient catalysts for light driven hydrogen evolution. Seeded CdSe@CdS nanorods have shown increasing performance with increasing rod length. This observation was rationalized by the increasing lifetime of the separated charges, as a large distance between holes localized in the CdSe seed and electrons localized at the metal tip decreases their recombination rate. However, the impact of nanorod length on electron-to-tip localization efficiency or pathway remained an open question. Therefore, we investigated the photo-induced electron transfer to the metal in a series of Ni tipped CdSe@CdS nanorods with varying length. We find that the transfer processes occurring from the region close to the semiconductor-metal interface, the rod region, and the CdSe seed region depend in different ways on the rod's length. The rate of the fastest process from excitonic states generated directly at the interface is independent of the rod length but the relative amplitude decreases with increasing rod length as the weight of the interface region is decreasing. The transfer of electrons to the metal tip from excitons generated in the CdS rod region depends strongly on the length of the nanorods which indicates an electron transport limited process, i.e., electron diffusion towards the interface region followed by fast interface crossing. The transfer originating from CdSe excitonic states again shows no significant length dependence in its time constant as it is probably limited by the rate of overcoming the shallow confinement in the CdSe seed.

INTRODUCTION

Semiconductor-metal hybrid nanostructured photocatalytic systems have been the focus of intense research due to their ability to support solar-to-fuel conversion.[1–5] In such hybrid systems, the semiconductor nanoparticle serves as a light-harvester, which transfers an electron to a metallic cocatalyst upon photoexcitation. Understanding the underlying charge carrier dynamics within the complete system is crucial for developing improved systems. In particular, the influence of the metal cocatalyst composition,[6–11] size,[12–15] deposition site, and particle number[16–20] on the interfacial charge transfer and resulting photon-to-hydrogen efficiency has been investigated in detail during the past years. In comparison, charge carrier migration within the semiconductor component has received little attention. It is well established for pure one-dimensional semiconductor systems that the semiconductor dimensions and surface quality influence the charge migration and localization.[21–25] However, the influence of these intrinsic charge carrier migration dynamics on the charge separation dynamics and efficiency in hybrid systems remains a relatively unexplored topic.

Hybrid systems, comprised of CdSe@CdS dot-in-rod particles functionalized with metallic nanoparticles, demonstrated high efficiency in converting protons to molecular hydrogen upon photoexcitation.[2,26,27] We previously found that the rate constant of electron transfer to the metal cocatalyst in such systems was independent with respect to metal size[12] or composition,[7] whereas the charge separation and photocatalytic hydrogen production efficiency were highly sensitive to these parameters. In general, electron transfer in these hybrid systems originates from excitons localized at different locations within the rod, i.e., near the interface, near the CdSe core, or within the core, and occurs within ~100 ps.[7,12,28] In contrast, the interface crossing from the semiconductor to the metal domain is expected to be much faster (< 1 ps).[15,29] The independence of the observed electron transfer rate constant from the characteristics of the metal cocatalyst can thus be explained by a slower electron diffusion towards the tip, which precedes any interface crossing and determines the observed rate, whereas the efficiency of interface crossing determines the catalytic efficiency.

Herein we provide evidence that intra-rod electron diffusion can be the rate-determining step for electron transfer. We have investigated seeded nanorods of similar diameter (5.0 ± 0.4 nm) and identical metal cocatalyst composition and size (Ni, 5.0 ± 0.5 nm) while varying the rods' length in the range of 20 – 60 nm. We used transient absorption spectroscopy to follow the photoinduced bleach recovery and electron dynamics and determined how the electron transfer kinetics develops as a function of the rod's length. We discuss the implications of these findings for the future design of optimized nanoscale photocatalytic hybrid systems.

RESULTS

Given the established influence of the rod's diameter and metal size[12,22,30] on the electronic structure and charge separation dynamics, respectively, it was vital to precisely control these characteristics, to enable proper studies on length dependent effects. The full protocols for CdSe@CdS rod synthesis and Ni tipping are published elsewhere,[12,26] and a full account of the synthetic protocols is included in the supporting information. Nanorods with varied length were obtained via adjustment of the amounts of CdSe seed and ligands that were used in their synthesis. Alternative methods for length adjustments such as variations in reaction temperature or reaction time were avoided, in an attempt to fix the rods' diameter. The well-controlled deposition of a Ni nanoparticle tip is based on the reduction of nickel(II) acetylacetonate as the nickel precursor by oleylamine and trioctyl phosphine.[10] Adjustments of the nickel precursor concentration, reaction temperature and time, and the ligands which are used enables the desired control over the Ni nanoparticle size, location, and number of sites on the CdS rod surface. The Ni tip size was selected to be 5.0 ± 0.5 nm, given that this size displayed the optimal photocatalytic activity towards hydrogen production.[12] Figure 1 shows transmission electron microscope (TEM) micrographs of the examined rods, with similar diameter and Ni tip size, and varying lengths. The detailed information on the dimensions (length, width, Ni-tip diameter) as well as statistics for the number of metal domains per rod is included in Table 1. The samples were given abbreviated names, representing the rods length, which are used throughout the paper (Table 1).

Absorption spectra of all pure nanorods dispersed in toluene showed the characteristic excitonic transitions related to the CdS rod below 470 nm and the comparably minor CdSe seed absorption at c. 560 nm (Figure S6).[31,32] The ratio of CdS:CdSe absorption becomes larger with increasing rod length because of the increasing CdS rod volume. Ni-tipped samples show additional broad absorption contribution spanning the entire visible spectrum due to scattering and absorption of light by the Ni nanoparticles (Figure 1f).

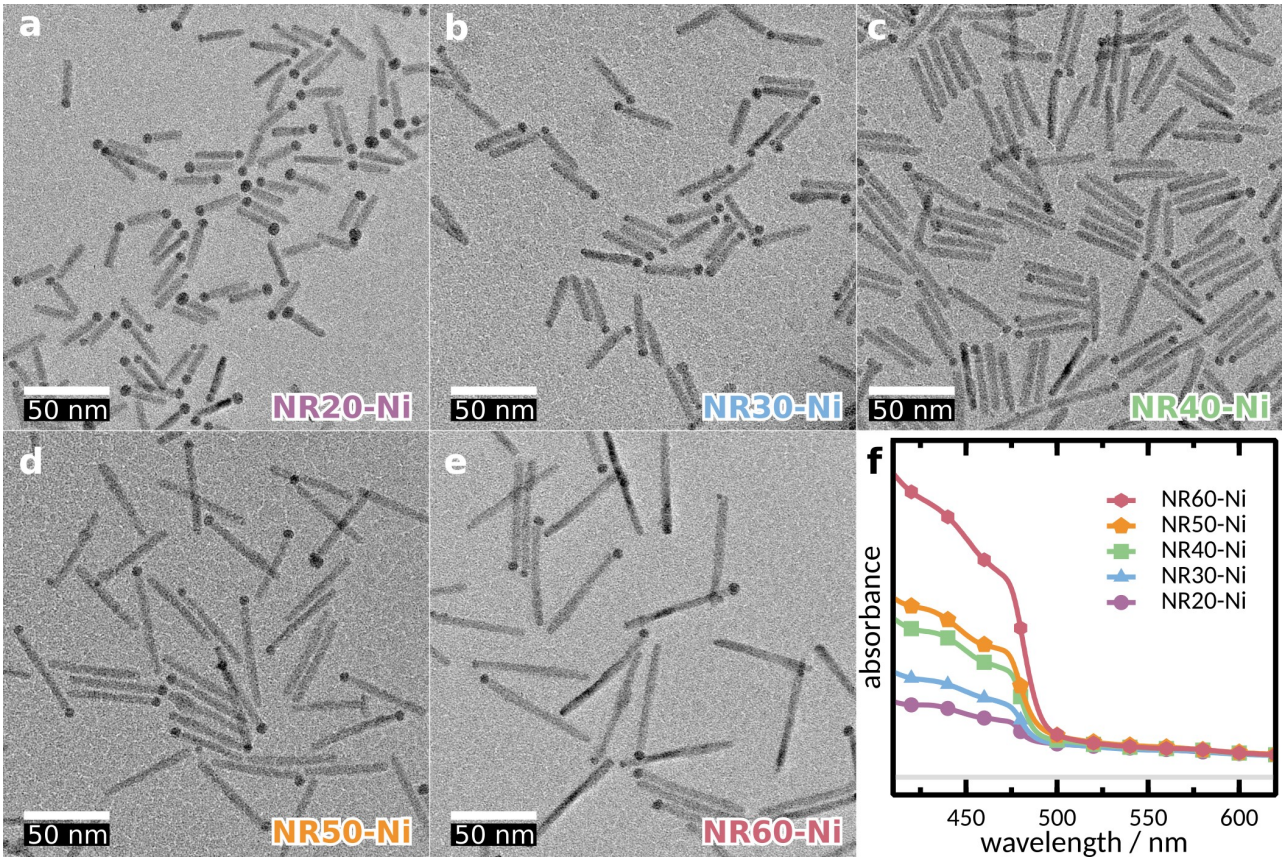

Figure 1. Characterization of Ni-tipped CdSe@CdS nanorods. (a) - (e) TEM micrographs of the structures under investigation. (f) Absorption spectra of tipped nanorods. All spectra have been normalized to the tip absorption at 650 nm. TEM images and absorption spectra of non-functionalized samples can be found in the Supporting Information.

Table 1. Overview of investigated CdSe@CdS nanorods. Indicated are the rod length and width as well as the Ni-tip diameter. For the tipped samples, we also indicated the amount of untipped (0T), single-tipped (1T), and double-tipped (2T) rods present in the sample mixture.

Bare sample	Length / nm	Width / nm	Ni-tipped samples	Tip diameter/ nm (0T-1T-2T / %)
NR20	19.7 ± 1.6	5.0 ± 0.4	NR20-Ni	4.7 ± 0.3 (3-88-9)
NR30	30.0 ± 2.0	5.4 ± 0.5	NR30-Ni	4.5 ± 0.6 (10-83-7)
NR40	40.1 ± 3.1	5.3 ± 0.6	NR40-Ni	4.8 ± 0.5 (12-82-6)
NR50	51.5 ± 3.5	4.6 ± 0.5	NR50-Ni	4.8 ± 0.6 (13-82-6)
NR60	60.7 ± 4.6	5.4 ± 0.5	NR60-Ni	5.5 ± 0.8 (20-80-1)

Photoluminescence spectroscopy gives first insights into the nanorod-tip interaction. For the bare nanorods, we observe the band-edge emission of the CdSe core (recorded upon excitation of the CdS rod at 450 nm) between 530 and 630 nm (Figure S7). Absolute photoluminescence quantum yields of bare rods are in the order of 0.5 - 0.8 (Table S2). Photoluminescence spectra of Ni-tipped samples are identical to their respective bare samples, but their quantum yields are drastically reduced to 0.1 and less. We attribute part of this residual emission to untipped nanorods, which are sometimes present in quantitative amounts (up to 20 % for NR60-Ni) together with the tipped samples. Additionally, some residual emission that originates from metal tipped rods provides an inverse indication of the efficiency of interfacial charge crossing.[12,33] Given the optimization of the Ni domain size, which was designed to maximize the probability for charge separation, the contribution to the emission by metal tipped rods, in this case, is minimal. Indeed, once we correct for the fraction of non-functionalized nanorods, the quenching efficiency for all tipped rods is close to unity (see SI for a detailed description). This confirms that charge-separation of the photogenerated exciton competes very efficiently with radiative recombination: while the hole ultimately localizes to the CdSe core, the electron is transferred to the Ni tip.[12,34]

Charge transfer to the cocatalyst in metal-semiconductor hybrid systems occurs within several 10s of picoseconds and faster. Thus, we investigated charge separation kinetics on a sub-2-ns-timescale via transient absorption spectroscopy with sub-100-fs time resolution. Transient absorption spectroscopy is sensitive to the population of conduction band states in photoexcited nanostructures and delivers information on electron dynamics.[22,31,35] Samples were excited at 390 nm, i.e., the CdS rod, and probed with a supercontinuum spanning from 350 to 750 nm. Transient spectra recorded for bare nanorods show the characteristic bleach features of the CdS rod excitonic transition between 460-480 nm and the CdSe core excitonic transition between 530-600 nm, due to state filling of the conduction band levels (Figure S8 – S12).[36] As expected, the CdS bleach recovery is substantially accelerated in the Ni functionalized samples, compared to bare samples (Figure 2a) and is complete within several hundred ps. We assign the accelerated bleach recovery to the interfacial electron transfer from the CdS rod conduction band to the Ni tip.

To gain a quantitative understanding of the temporal and spectral evolution of the transient spectra, they were subjected to a global fit. Our model accounts for the presence of bare rods together with the tipped rods (see Table 1) and for tipped nanorods that do not undergo charge separation.[12,37] In the region of 400-500 nm, reflecting on the bleach of CdS localized excitonic transitions, we modeled the accelerated bleach recovery of tipped rods with two time constants ($\tau_{ET,1}$ and $\tau_{ET,2}$), which reflect the electron transfer to the Ni tip. In addition, we separately modeled the CdS bleach dynamics in non-functionalized samples

by four time constants (Table 2). A complete discussion of these time constants for non-functionalized samples can be found in the Supporting Information. In the following we solely focus on the discussion of the length dependence of the electron transfer process.

The first time constant $\tau_{ET,1}$ is for the functionalized samples in the order of 0.2 ps for all samples, irrespective of their length. A similarly fast process on a timescale of 100s of fs has previously been observed for metal-tipped CdSe@CdS, CdSe, and CdS nanorods,[15,28,29] and has been attributed to a "hot" electron transfer. In such case, the electron transfer to the tip precedes any intra-band relaxations to the band-edge. The second time constant $\tau_{ET,2}$ is in the order of few to 10s of ps and corresponds to band-edge electron transfer to the Ni tip.[12] As clearly seen in Figure 2b, $\tau_{ET,2}$ increases with increasing rod length from $\tau_{ET,2}$ = 7.6±2.4 ps for the NR20-Ni sample to $\tau_{ET,2}$ = 29.6±5.7 ps for NR60-Ni. Electron transfer in NR50-Ni was found to be substantially faster than expected from the trend given by the other samples. This deviation from the general trend may be ascribed to the nanorod width, which is smaller than that of the other nanorods. The CdS diameter affects the intrinsic underlying electronic structure of the nanorod and, accordingly, the electron dynamics.[30]

The accelerated CdSe bleach decay was quantified in the spectral region of 530 – 610 nm in a similar manner. Here, a single time constant was required to describe the accelerated decay compared to the bare rods, and without considerable changes between samples. It was determined to be in the order of $\tau_{ET,CdSe}$ = (60 ± 10) ps. Again, NR50-Ni showed a faster bleach recovery, presumably due to its smaller width. In quasi-type II nanostructures, the electron is delocalized over the entire structure, yet with higher probability around the CdSe core. Hence, the CdSe bleach is representative of the conduction band electron population situated close to, and in, the core. The time constant $\tau_{ET,CdSe}$ thus represents electron transfer from excitonic states localized in or near the CdSe seed.[12]

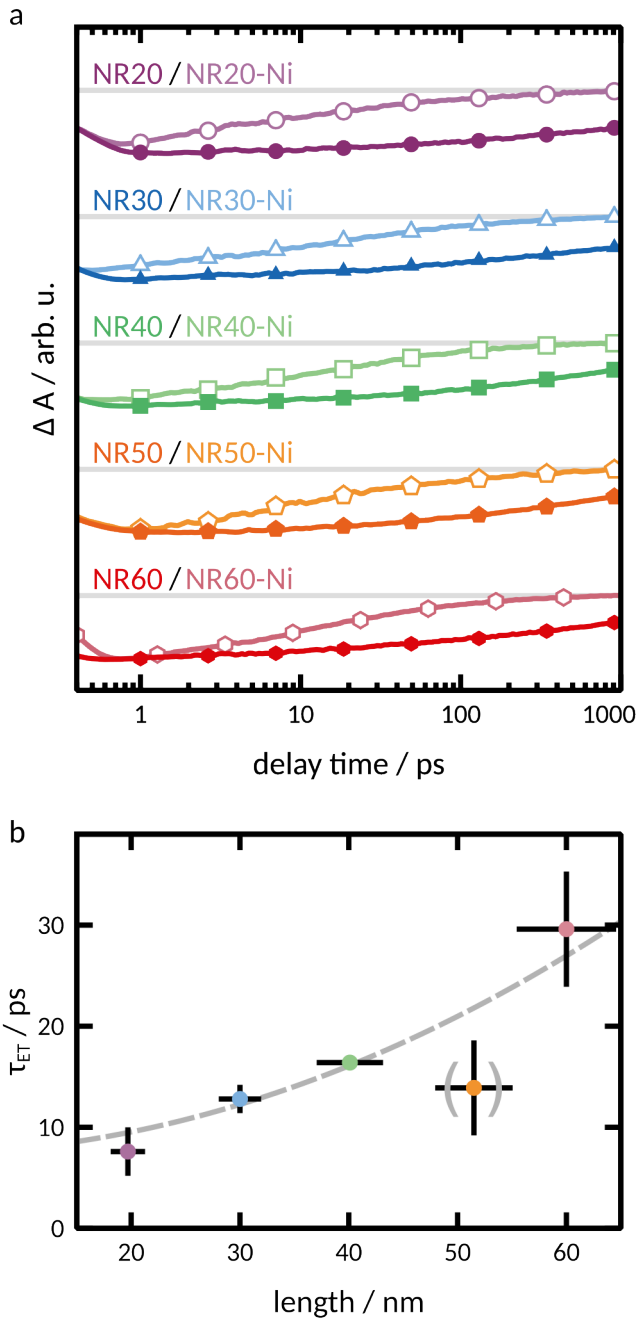

Figure 2. Transient absorption spectroscopy of pure and hybrid structures. (a) Normalized kinetics of CdS bleach recovery at 460 nm of bare (filled symbols) and functionalized (open symbols) nanorods. To obtain pure kinetic traces for functionalized nanorods without contributions of residual bare rods, bare nanorod kinetics normalized at 1000 ps was subtracted from the as-measured kinetics of functionalized samples. (b) Determined CdS conduction band electron transfer lifetimes ($\tau_{ET,2}$) as a function of rod length. The dashed line represents a quadratic fit of the data excluding NR50-Ni.

Table 2. Time-constants of electron transfer in tipped CdSe@CdS obtained *via* global fitting of the CdS and CdSe bleach regions. Time constants of non-functionalized nanorods can be found in the Supporting information (Tables S3 and S4).

Sample	$\tau_{ET,1}$ / ps	$\tau_{ET,2}$ / ps	$\tau_{ET,CdSe}$ / ps
NR20-Ni	0.3±0.1	7.6±2.4	45±17
NR30-Ni	0.2±0.1	12.8±1.4	59±4
NR40-Ni	0.3±0.1	16.4±0.7	71±10
NR50-Ni	0.3±0.1	11.7±0.9	25±11
NR60-Ni	0.2±0.1	29.6±5.7	54±4

DISCUSSION

The goal of this study was to shed light on the electron transfer mechanism in 1-dimensional semiconductor-metal hybrid systems. In accordance with previous literature reports, we identified three distinct time regimes of electron transfer, which we can relate to the structure of the hybrid system. First, we observed a very fast ($\tau_{ET,1} << 1$ ps) hot electron transfer to the metal tip that is independent of the rod's length. We want to emphasize that the determined lifetime of $\tau_{ET,1}$ is limited by our experimental time resolution of ~100 fs. This process occurs on the same or even shorter timescale than the dissociation of the exciton that is followed by hole localization to the CdSe core (as indicated by τ_2 in the bare rods). Hence, we interpret this as interfacial electron transfer, occurring directly from a photogenerated exciton that is generated in the CdS rod in close proximity to the Ni tip. The time constant for such direct interfacial charge crossing is not expected to be sensitive to the rod's length, in accordance with our observations. An analysis of the corresponding amplitudes of both electron transfer steps shows that the relative contribution of this hot electron transfer to the bleach recovery varies and is inversely proportional to the rod length (Supporting Information). Additional influences which might be caused by varying barrier heights are related to changes in the nickel particle's size, and thus may be neglected here, given that all rods possess similar sized Ni tips. This amplitude accounts for ~70 % of the bleach recovery for NR20-Ni and drops to ~50 % for NR60-Ni. These trends further support our assignment of $\tau_{ET,1}$ to the interfacial electron transfer, as this process becomes more probable with a shorter distance from the location of exciton formation to the metal tip. In other words, with decreasing rod's length the probability of photogeneration of an exciton in sufficient proximity to the interface increases.

On the other hand, the band-edge electron transfer (as expressed in $\tau_{ET,2}$) in the order of several ps becomes slower with increasing rod length, which indicates that electron diffusion to the metal tip is the rate determining step in this charge transfer process. The relationship between $\tau_{ET,2}$ and the rod's length is successfully approximated with a quadratic fit, which represents the one-dimensional electron diffusion,[22] and yields a diffusion constant in the order of $\sim 10^{-4}$ m^2 s^{-1}. Even though our simplistic approach ignores additional electron decay pathways such as localization or trapping, which may occur on a similar timescale, this value is in good accordance with the determined value for electron diffusion in non-functionalized CdSe@CdS nanorods of 2.4×10^{-4} m^2 s^{-1}.[22] While this estimation for non-functionalized rods is based on localization efficiencies derived from steady-state photoluminescence spectroscopy, the diffusion constant obtained for Ni-tipped rods in the present work stems from actual fitting of time constants.

Finally, we observed the transfer of electrons, which are situated near the CdSe core, and whose time constant $\tau_{ET,CdSe}$ (~60 ± 10 ps) is again independent of the rod's length. For all samples investigated, this process is significantly slower than the diffusion-controlled band-edge electron transfer ($\tau_{ET,2}$). Because the metal particle preferentially grows at the (001) facet of the CdS rod,[38] i.e., the rod tip farthest away from the CdSe seed,[39] it is surprising that $\tau_{ET,CdSe}$ does not similarly depend on the rod dimensions as does $\tau_{ET,2}$. A plausible explanation for this result is that overcoming the shallow confinement of the electron to the CdSe core region, due to the rod's quasi-type II electronic structure, is the rate-determining step in this electron transfer process, whereas the diffusion towards the tip is relatively faster in this case. These results manifest into generalized design principles for one-dimensional photocatalytic semiconductor-metal systems. Interfacial electron crossing to the metal catalyst is significantly faster than any electron diffusion and is not the rate-determining step for charge separation. Yet, we found that the relative efficiency of interfacial hot electron transfer slightly decreases with increasing rod's length. In contrast, band-edge electron transfer is highly sensitive to the nanorod's dimensions. Song et al. recently emphasized the complicated relation between reduced electron transfer rates and increased absorption coefficients with increasing rod length in Pt-tipped CdSe nanorods.[40] They deduced an optimal nanorod length of ~20 nm; a length scale at which dot-in-rod hybrid systems perform worse than pure nanorods.[28,41] On the other hand, CdSe@CdS-Pt nanorods showed significantly improved hydrogen generation quantum efficiency upon increasing the rod's length from 20 nm to 70 nm.[42] Our findings deliver a mechanistic explanation for this. Even though band-edge electron transfer is diffusion controlled, electron diffusion to the semiconductor-metal interface is still sufficiently fast to outcompete recombination processes up to lengths of at least 60 nm and hence is not limiting the electron transfer to the metal tip. Wu *et al.* previously estimated the optimal rod length for photocatalysis to be ~100 nm

based on the rod-to-seed localization efficiency in non-functionalized dot-in-rods.[22] Extrapolation of electron transfer times in Figure 2b to this rod length yields an electron transfer time constant of ~70 ps (see SI for details), which is still substantially faster than other electron trapping and recombination pathways. Electron diffusion accordingly still occurs efficiently even at such long lengths. This emphasizes the integral role of the dot-in-rod design investigated here, in which the CdSe seed supports orders of magnitude longer electron-hole separation than for unseeded rods.[7,43]

In short, we presented a simple framework for optimized semiconductor-metal hybrid nanostructured photocatalytic system design towards efficient photocatalytic reactions such as water splitting.

SUPPORTING INFORMATION

Supporting Information includes detailed information of the synthetic protocols and sample characterization with information on the methodologies utilized. The Supporting Information is available free of charge on the website.

ACKNOWLEDGMENT

This research was supported, in part, by a grant from the German-Israeli Foundation for Scientific Research and Development (GIF, grant number G-1535-500.15/2021). Further the financial support by the German Research Foundation (DFG) under Project No. 364549901 – TRR234 (CataLight, B4) and the Fonds der Chemischen Industrie (FCI) is acknowledged (MW). LA and KD acknowledge the support of Marie Sklodowska-Curie Actions of the European H2020 programme MSCA-ITN-2016 (G.A No: 722591 - PHOTOTRAIN), and the support of the Israeli Ministry of National Infrastructures, Energy and Water Resources (grant number 218-11-044).

AUTHOR DECLARATION

The authors have no conflicts to disclose.

AUTHOR CONTRIBUTIONS

Mathias Micheel: Conceptualization, Data curation, Formal analysis, Investigation, Methodology, Validation, Visualization, Writing – original draft, Writing – review & editing. **Kaitou Don**g: Conceptualization, Formal analysis, Investigation, Methodology. **Lilac Amirav**: Conceptualization, Data curation, Funding acquisition, Methodology, Project administration, Resources, Supervision, Writing – review & editing. **Maria Wächtler**: Conceptualization, Data curation, Formal analysis, Funding acquisition, Methodology, Project administration, Resources, Supervision, Writing – original draft, Writing – review & editing.

DATA AVAILABILITY

Spectroscopic data, including absorption, photoluminescence, and transient absorption spectroscopy that support the findings of this study are openly available in Zenodo at http://doi.org/[doi], reference number [reference number].

REFERENCES

[1] N. Waiskopf, Y. Ben-Shahar, and U. Banin, Advanced Materials **30**, 1706697 (2018).

[2] K. Wu and T. Lian, Chem. Soc. Rev. **45**, 3781 (2016).

[3] R. Burke, K.L. Bren, and T.D. Krauss, J. Chem. Phys. **154**, 030901 (2021).

[4] P. Moroz, A. Boddy, and M. Zamkov, Frontiers in Chemistry **6**, (2018).

[5] N. Razgoniaeva, P. Moroz, S. Lambright, and M. Zamkov, J. Phys. Chem. Lett. **6**, 4352 (2015).

[6] P. Kalisman, L. Houben, E. Aronovitch, Y. Kauffmann, M. Bar-Sadan, and L. Amirav, J. Mater. Chem. A **3**, 19679 (2015).

[7] M. Wächtler, P. Kalisman, and L. Amirav, J. Phys. Chem. C **120**, 24491 (2016).

[8] K. Dong, Q.-C. Chen, Z. Xing, Y. Chen, Y. Qi, N.G. Pavlpoulos, and L. Amirav, Chem. Mater. **33**, 6394 (2021).

[9] E. Aronovitch, L. Houben, and M. Bar-Sadan, Chemistry of Materials (2019).

[10] Y. Nakibli and L. Amirav, Chem. Mater. **28**, 4524 (2016).

[11] E. Aronovitch, P. Kalisman, S. Mangel, L. Houben, L. Amirav, and M. Bar-Sadan, J. Phys. Chem. Lett. **6**, 3760 (2015).

[12] Y. Nakibli, Y. Mazal, Y. Dubi, M. Wächtler, and L. Amirav, Nano Lett. **18**, 357 (2018).

[13] Y. Liu, W. Yang, Q. Chen, D.A. Cullen, Z. Xie, and T. Lian, J. Am. Chem. Soc. **144**, 2705 (2022).

[14] Y. Ben-Shahar, F. Scotognella, I. Kriegel, L. Moretti, G. Cerullo, E. Rabani, and U. Banin, Nature Communications **7**, 10413 (2016).

[15] Y. Ben-Shahar, J.P. Philbin, F. Scotognella, L. Ganzer, G. Cerullo, E. Rabani, and U. Banin, Nano Lett. **18**, 5211 (2018).

[16] T. Simon, M.T. Carlson, J.K. Stolarczyk, and J. Feldmann, ACS Energy Lett. **1**, 1137 (2016).

[17] Y. Nakibli, P. Kalisman, and L. Amirav, J. Phys. Chem. Lett. **6**, 2265 (2015).

[18] J.U. Bang, S.J. Lee, J.S. Jang, W. Choi, and H. Song, J. Phys. Chem. Lett. **3**, 3781 (2012).

[19] M. Karakus, Y. Sung, H.I. Wang, Z. Mics, K. Char, M. Bonn, and E. Cánovas, J. Phys. Chem. C **121**, 13070 (2017).

[20] Y. Sung, J. Lim, J.H. Koh, L.J. Hill, B.K. Min, J. Pyun, and K. Char, CrystEngComm **17**, 8423 (2015).

[21] M. Micheel, B. Liu, and M. Wächtler, Catalysts **10**, 1143 (2020).

[22] K. Wu, L.J. Hill, J. Chen, J.R. McBride, N.G. Pavlopolous, N.E. Richey, J. Pyun, and T. Lian, ACS Nano **9**, 4591 (2015).

[23] M.D. Peterson, L.C. Cass, R.D. Harris, K. Edme, K. Sung, and E.A. Weiss, Annual Review of Physical Chemistry **65**, 317 (2014).

[24] V.L. Bridewell, R. Alam, C.J. Karwacki, and P.V. Kamat, Chem. Mater. **27**, 5064 (2015).

[25] K. Wu, W. Rodríguez-Córdoba, and T. Lian, J. Phys. Chem. B **118**, 14062 (2014).

[26] P. Kalisman, Y. Nakibli, and L. Amirav, Nano Lett. **16**, 1776 (2016).

[27] A. Agosti, Y. Nakibli, L. Amirav, and G. Bergamini, Nano Energy **70**, 104510 (2020).

[28] K. Wu, Z. Chen, H. Lv, H. Zhu, C.L. Hill, and T. Lian, J. Am. Chem. Soc. **136**, 7708 (2014).

[29] F.V.A. Camargo, Y. Ben-Shahar, T. Nagahara, Y.E. Panfil, M. Russo, U. Banin, and G. Cerullo, Nano Lett. **21**, 1461 (2021).

[30] T. Rosner, N.G. Pavlopoulos, H. Shoyhet, M. Micheel, M. Wächtler, N. Adir, and L. Amirav, Nanomaterials **12**, 3343 (2022).

[31] K. Wu, W.E. Rodríguez-Córdoba, Z. Liu, H. Zhu, and T. Lian, ACS Nano **7**, 7173 (2013).

[32] M.G. Lupo, F. Della Sala, L. Carbone, M. Zavelani-Rossi, A. Fiore, L. Lüer, D. Polli, R. Cingolani, L. Manna, and G. Lanzani, Nano Lett. **8**, 4582 (2008).

[33] L. Amirav and A.P. Alivisatos, J. Am. Chem. Soc. **135**, 13049 (2013).

[34] M. Zhukovskyi, P. Tongying, H. Yashan, Y. Wang, and M. Kuno, ACS Catal. **5**, 6615 (2015).

[35] D.P. Morgan and D.F. Kelley, J. Phys. Chem. C **124**, 8448 (2020).

[36] Q. Li, W. Yang, and T. Lian, in *Springer Handbook of Inorganic Photochemistry*, edited by D. Bahnemann and A.O.T. Patrocinio (Springer International Publishing, Cham, 2022), pp. 985–1012.

[37] A. Schleusener, M. Micheel, S. Benndorf, M. Rettenmayr, W. Weigand, and M. Wächtler, J. Phys. Chem. Lett. **12**, 4385 (2021).

[38] S.E. Habas, P. Yang, and T. Mokari, J. Am. Chem. Soc. **130**, 3294 (2008).

[39] D.V. Talapin, J.H. Nelson, E.V. Shevchenko, S. Aloni, B. Sadtler, and A.P. Alivisatos, Nano Lett. **7**, 2951 (2007).

[40] J.Y. Choi, W.-W. Park, B. Park, S. Sul, O.-H. Kwon, and H. Song, ACS Catal. **11**, 13303 (2021).

[41] F. Qiu, Z. Han, J.J. Peterson, M.Y. Odoi, K.L. Sowers, and T.D. Krauss, Nano Lett. **16**, 5347 (2016).

[42] L. Amirav and A.P. Alivisatos, J. Phys. Chem. Lett. **1**, 1051 (2010).

[43] K. Wu, H. Zhu, Z. Liu, W. Rodríguez-Córdoba, and T. Lian, J. Am. Chem. Soc. **134**, 10337 (2012).